

Applied Superconductivity II, SS 2002

Lesson # 5 Accelerator Magnets

Luca Bottura
CERN Division LHC
CH-1211 Geneva 23, Switzerland
Luca.Bottura@cern.ch

Accelerator principles

Particle accelerators are one of the main tools of nuclear physics. Accelerator research is usually carried out smashing high energy particles against targets (fixed targets experiments), or against each other (collider experiments). The products of the interactions depend on the nature and energy of the particles flying in the accelerator. In general higher particle energy is associated with higher resolution, much as a microscope resolution increases with the reduction of the wavelength of the light used to illuminate the object.

The present state of the art for the energy of a single particle in an accelerator is 1 TeV ($1.6 \cdot 10^{-7}$ J) provided by the Tevatron complex at FNAL. CERN is presently building the Large Hadron Collider (LHC), that will provide towards the end of the first decade of 2000 counter-rotating protons with energy nearly one order of magnitude higher, 7 TeV, and 14 TeV in the center of mass of two colliding protons. At this energy level the particles are highly relativistic. Figure 1 shows the so called Livingston chart with the evolution of the accelerator energy in time and as a function of the evolving accelerator technology.

Modern accelerators are of two main types: linear accelerators (also referred to as *linacs*) and circular accelerators. Linear accelerators (see Fig. 2) consist of a sequence of accelerating cavities where a suitable electric field accelerates the particles and focussing elements that eventually produce a small, high energetic beam emerging at the end of the accelerator. In linacs the maximum particle energy is determined by the product of number and strength of accelerating stations. For a given accelerating strength this product corresponds to length of the accelerator that is generally limited by practical considerations and cost.

Circular accelerators (see Fig. 3) consist of accelerating cavities and guiding magnets with uniform field that bend the beam on a closed orbit, eventually bringing it back to the accelerating station. The advantage of this type of accelerators is that the beam can be accelerated in small quanta at each passage and in the absence of losses the maximum energy that can be reached does not depend on the number and strength of accelerating stations.

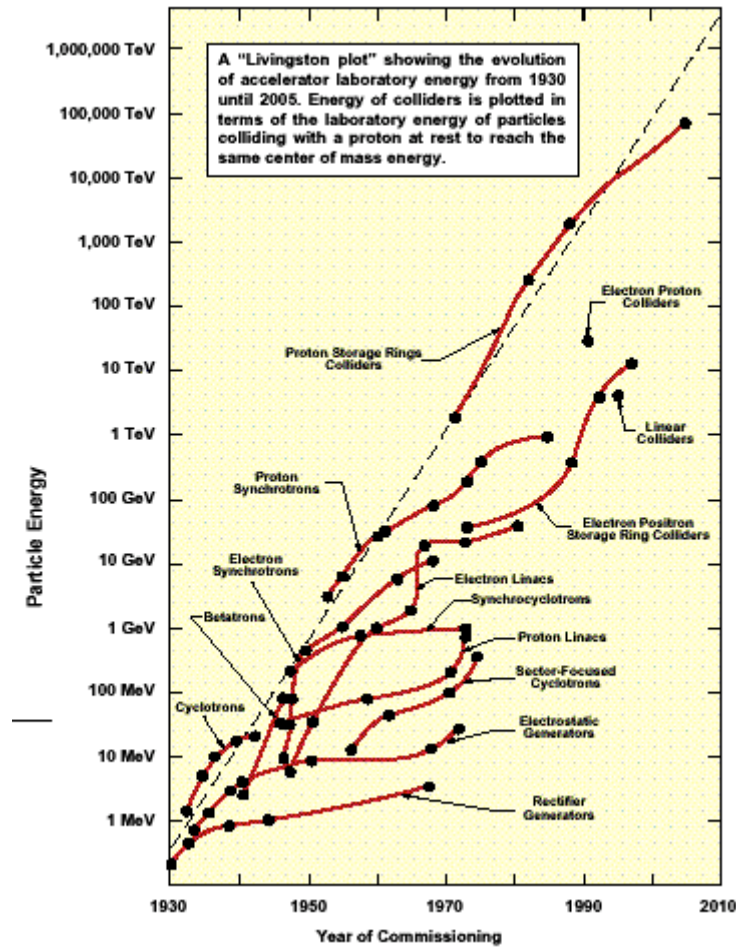


Figure 1. Livingston chart for modern accelerators. The time scale is the year of completion of the accelerator, the vertical scale is the equivalent energy of particles in a beam colliding with a proton at rest that has the same center of mass energy.

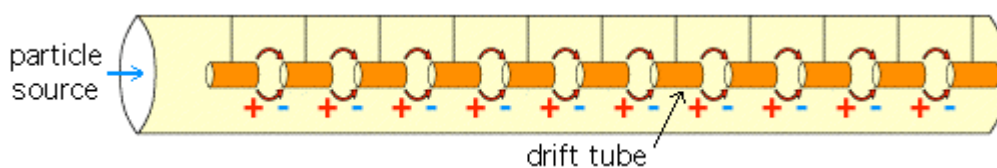


Figure 2. Principle of a linear accelerator.

In circular accelerators the maximum beam energy is limited by two processes. On one side the beam bending radius ρ in the guiding magnets depends on the beam energy E and on the magnetic field B :

$$\rho[m] = \frac{E[\text{GeV}]}{0.3qB[\text{T}]}$$

where the energy E is in units of [GeV], the particle charge q is in units of electron charge and the magnetic field B is in units of [T]. As an example a 1 TeV ($E=1000$ GeV) proton ($q=1$) is bent by a 5 T field on a radius $\rho = 667$ m. In practice the

magnetic field that can be produced is limited whatever the technology used (permanent magnets, classical or superconducting electromagnets), hence the accelerator size grows linearly with the maximum beam energy.

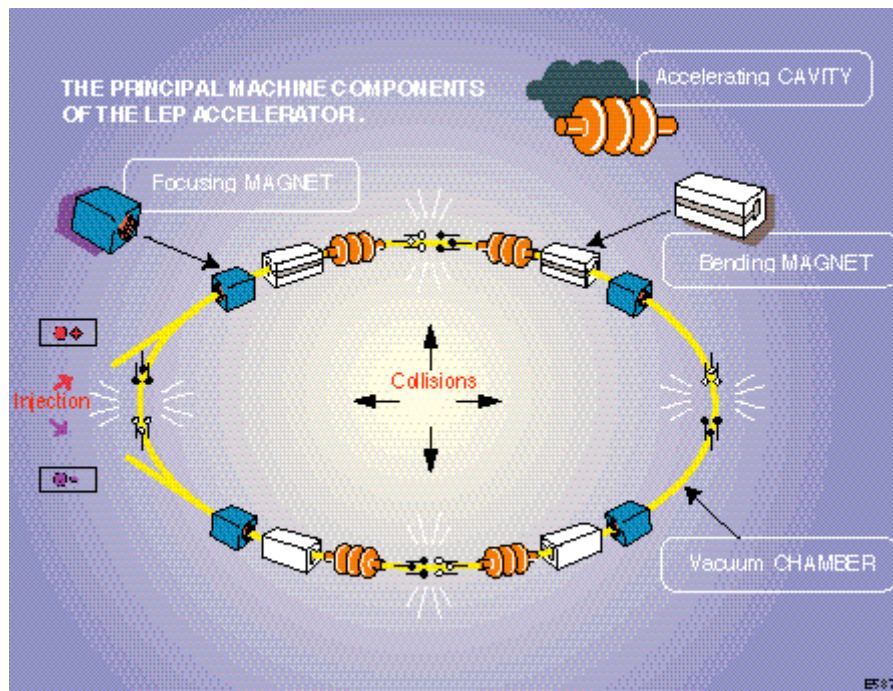


Figure 3. Principle of a circular accelerator (shown here for the case of the Large Electron Positron collider, LEP).

On the other side a particle on a bent trajectory emits synchrotron radiation and thus loses energy. The energy lost δE per turn in the accelerator is given by:

$$\delta E [\text{keV}] = 88.5 \frac{E^4 [\text{GeV}]}{\rho [\text{m}]} \frac{1}{m^4}$$

where m is the rest mass of the particle in units of the electron mass at rest, and the energy E is again in units of [GeV]. As an example a proton ($m = 1840$) with an energy of 1 TeV ($E=1000$ GeV) and bent on the curvature radius found above, $\rho = 667$ m, would lose an energy of $\delta E = 0.012$ keV per turn.

The energy lost per turn decreases with the fourth power of the rest mass of the particle. For comparison, an electron ($m = 1$) with the same energy and on the same curvature radius would lose ideally an astronomic amount of energy $\delta E = 1.3 \cdot 10^{11}$ keV per turn, corresponding to 130 TeV, a factor 10^{13} larger than in the case of a proton. This is the reason why modern circular accelerators use heavy particles (to minimise energy loss), while synchrotron radiation sources use electrons (to maximise radiation). We also see that the energy lost per turn increases with the fourth power of the energy. At a given point the energy replenishment at the accelerating cavity is equal to the energy lost in one turn along the accelerator and the limit is reached.

Exercise – plot the cost function obtained as a linear combination of civil engineering costs (proportional to the length), magnetic system cost (proportional to the length and the magnetic field) and power installed for acceleration and operation (proportional to the energy loss per turn):

$$C = C_1 \rho + C_2 \rho B^n + C_3 \delta E$$

and study the behaviour as a function of the accelerator radius and field, at constant E . Show that an optimum can be found both with respect to the radius and to the field.

The cost function at constant energy can be written in terms of the radius only as follows:

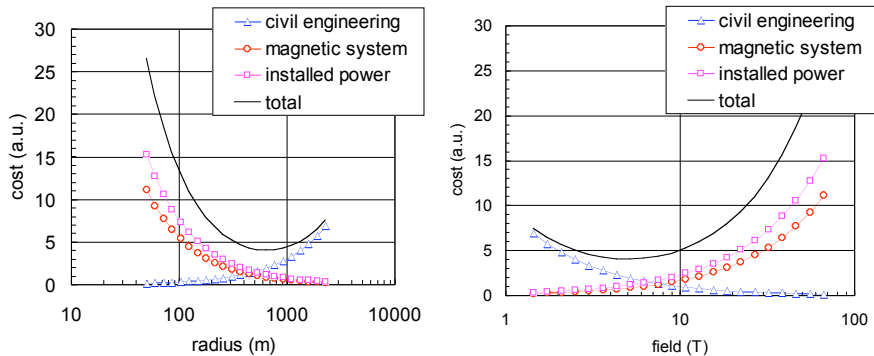
$$C = C_1 \rho + C_2 \rho \left(\frac{E}{0.3q\rho} \right)^n + 88.5C_3 \left(\frac{E}{m} \right)^4 \frac{1}{\rho}$$

and in terms of the field only as follows:

$$C = C_1 \frac{E}{0.3qB} + C_2 \frac{E}{0.3q} B^{n-1} + 88.5C_3 \frac{E^3}{m^4} 0.3qB$$

Below is a plot of the cost function and its contributions for the following choice of parameters:

$$C_1 = 3 \cdot 10^{-3}, C_2 = 5 \cdot 10^{-5}, C_3 = 8 \cdot 10^3, n = 2, q = 1, m = 1800, E = 1000 \text{ GeV}.$$

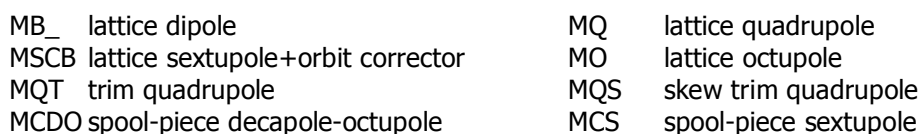


Circular accelerators are filled from an injector, that can also be a circular accelerator of smaller size. The beam is subsequently accelerated until it reaches the maximum energy and ejected into a following acceleration stage, into a target (fixed target operation) or stored until it is brought in collision with a counter-circulating beam at the experimental detectors (collider operation). In the operation of such a chain it is extremely important that the bending strength of the magnets tracks precisely the energy change of the beam during acceleration. This requirement of synchronicity is the reason why circular accelerators are often named *synchrotrons*.

In addition to bending the beam, the magnetic field is used in synchrotrons to focus the particle and thus maintain the beam size small. In the presence of a pure bending beam, perfectly homogeneous in space as shown in Fig. 4(a), particles in the beam with slight deviations from nominal conditions (small momentum or orbit errors) would spiral and drift away from the nominal orbit, eventually leaving the accelerator. This is avoided using gradient fields, such as shown in Fig. 4(b). A gradient field

Figure 1 consists of two parts. Part (a) shows a 1D chain of blue vertical arrows representing spins. A red dot representing an impurity is located between the fourth and fifth arrows. A red dashed arrow points from the impurity to the right. A coordinate system with x, y, and z axes is shown at the bottom. Part (b) shows a 2D chain of blue arrows. The arrows are arranged in a zigzag pattern along a diagonal line. Two red dots representing impurities are located at the ends of the chain. A red dashed arrow points from the left impurity to the right impurity. A coordinate system with x, y, and z axes is shown in the center.

This is the basic layout of a modern accelerator magnets, consisting of a regular repetition of cells of focussing magnets (indicated with the letter F), bending magnets (indicated with the letter O), defocussing magnets (indicated with the letter D) and bending magnets (O), or FODO. In addition to the magnets mentioned above, higher order gradient magnets are necessary to correct for the non-linear beam response to perturbations and to stabilize the beam. This is shown schematically in Fig. 5 that reports the structure of the basic cell of the LHC collider and includes all main correcting systems.



Because of their importance, this lecture focusses on superconducting accelerator magnets. Among the many aspects that are relevant for the design and construction, it

concentrates on the magnetic field and the influence of superconducting effects on the high field quality requested in accelerators.

Complex magnetic field notation for accelerator magnets

Magnets for accelerators are long and slender, and the field in the small bore can be considered with good approximation as purely 2-D. We can therefore concentrate on the cross section (x,y) and ignore the length z . With this assumption it is possible to use the complex notation first introduced by Beth [Beth-66, Beth-67] to simplify the mathematics. A function \mathbf{B} is defined in the current-free space from the two components of the field as follows:

$$\mathbf{B} = B_y + iB_x$$

where i is the imaginary unit, $\mathbf{s} = x + iy$ is the complex variable and $\mathbf{s}^* = x - iy$ is its complex conjugate. The complex function \mathbf{B} is analytic in the current-free space, as it satisfies the Cauchy-Riemann conditions:

$$\begin{aligned} \frac{\partial \operatorname{Re}(\mathbf{B})}{\partial x} - \frac{\partial \operatorname{Im}(\mathbf{B})}{\partial y} &= 0 \\ \frac{\partial \operatorname{Re}(\mathbf{B})}{\partial y} + \frac{\partial \operatorname{Im}(\mathbf{B})}{\partial x} &= 0 \end{aligned}$$

Exercise - prove that the function \mathbf{B} is analytic using the quasi-static Maxwell equations for linear materials $\nabla \times \mathbf{B} = \mu_0 \mathbf{J}$ and $\nabla \cdot \mathbf{B} = 0$.

We take the derivatives as needed and obtain:

$$\begin{aligned} \frac{\partial B_y}{\partial x} - \frac{\partial B_x}{\partial y} &= 0 \\ \frac{\partial B_y}{\partial y} + \frac{\partial B_x}{\partial x} &= 0 \end{aligned}$$

the first condition is true because the following equation holds in free space:

$$\nabla \times \mathbf{B} = 0$$

and the second condition is true because:

$$\nabla \cdot \mathbf{B} = 0$$

Since then \mathbf{B} is analytic, we can expand it in Taylor series around any point. Taking in particular the bore of the magnet and considering the disk that extends up to the first conductor, i.e. the current-free region, we can write that \mathbf{B} is given by the following series:

$$B_y + iB_x = \sum_{n=1}^{\infty} C_n \left(\frac{\mathbf{s}}{R_{ref}} \right)^{n-1}$$

where the complex coefficients C_n are the so called *harmonics* or *multipoles* of the field and R_{ref} is a reference radius chosen conveniently to scale the coefficients. The complex multipoles are written in terms of their real and imaginary parts:

$$C_n = B_n + iA_n$$

where the B_n are called the *normal* multipoles, while the A_n are the *skew* multipoles. The coefficients C_n , B_n and A_n are in units of T at the reference radius. A magnet is said to generate a pure normal or skew multipole of order m if the expansion of the field in the magnet bore contains only one coefficient B_m or A_m respectively. In particular a magnet with a field expansion containing only the term B_1 is said to generate a pure normal dipole field. The field in this case is given by:

$$B_y = B_1$$

it is constant and oriented along y and corresponds to the bending field examined above. If the only non-zero term is A_1 then the magnet is said to generate a pure skew dipole field, given by:

$$B_x = A_1$$

constant in space and oriented along y. A pure normal quadrupole field is obtained when the only non-zero coefficient is B_2 :

$$B_x = B_2 \frac{y}{R_{ref}} \quad B_y = B_2 \frac{x}{R_{ref}}$$

that corresponds to the gradient field examined above. If only A_2 is non-zero the field is then:

$$B_x = -A_2 \frac{x}{R_{ref}} \quad B_y = -A_2 \frac{y}{R_{ref}}$$

also called a skew quadrupole. The higher order terms are called by analogy normal and skew sextupole (B_3 and A_3 respectively), normal and skew octupole (B_4 and A_4), and so on.

It is normal practice in the measurement and analysis of the field to refer to normalised multipole coefficients, which we will indicate with lowercase letters:

$$c_n = b_n + ia_n$$

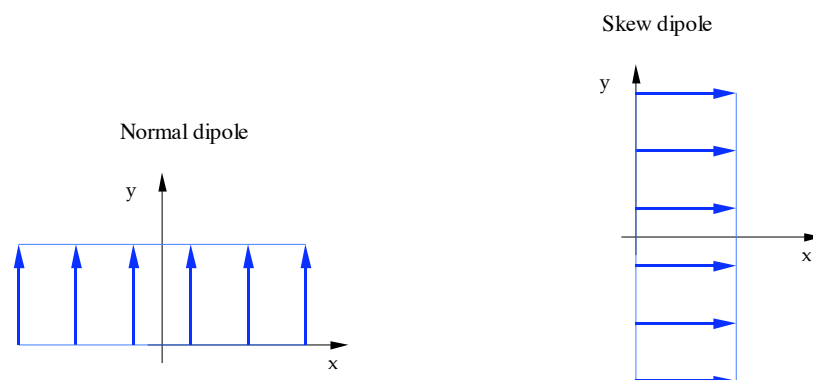
The normalised coefficients are obtained for a normal magnet of order m (recall that the dipole has $m = 1$) using:

$$\mathbf{c}_n = 10^4 \frac{C_n}{B_m} = 10^4 \left(\frac{B_n}{B_m} + i \frac{A_n}{B_m} \right) = b_n + ia_n$$

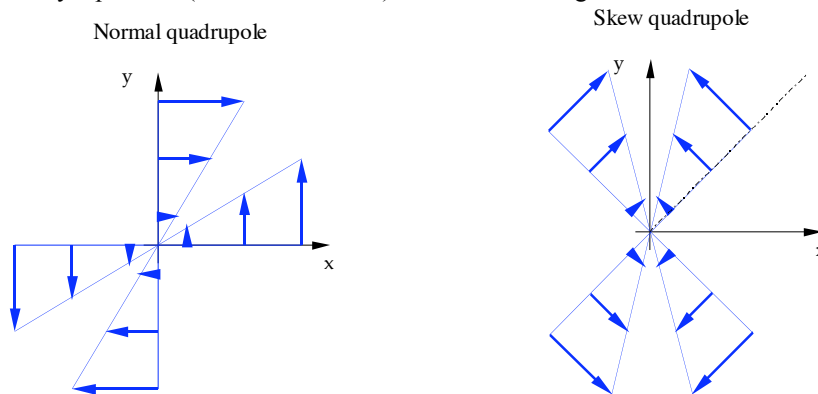
where the factor 10^4 is inserted for convenience, as higher order multipoles are generally small, typically of the order of 10^{-4} of the main field component. Although the normalised harmonic coefficient are dimensionless, they are usually quoted in so called *units*, a *unit* being the result of the normalization and scaling of the expression above.

Exercise – plot the field vectors for dipole, quadrupole and sextupole.

The normal and skew dipole B_1 and A_1 are a uniform field oriented along the y and x axes respectively



The normal quadrupole B_2 is a constant gradient field, oriented in y direction along the x axis and in x direction along the y axis. The skew quadrupole A_2 is obtained from the normal quadrupole by a positive (counterclockwise) rotation of 45 degrees.



Magnetic field of elementary current and moments

Magnetic field can be generated either flowing electric current in a conductor, or magnetizing suitable material. Both techniques are used for accelerator magnets. It is hence necessary to know the field generated by an elementary current and magnetic moment. The field generated at a location \mathbf{s} by a line of current I flowing in z direction and located at a position $\mathbf{R} = R_x + i R_y$ in complex plane is given by:

$$\mathbf{B} = \frac{\mu_0 I}{2\pi} \frac{1}{\mathbf{s} - \mathbf{R}}$$

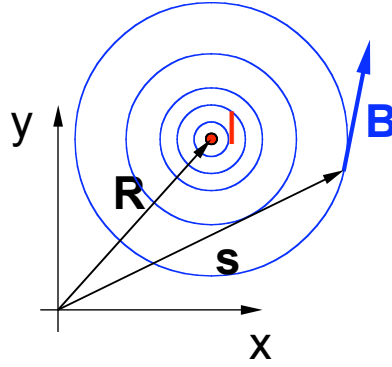


Figure 6. Field produced by a current line I placed at a position \mathbf{R} in complex plane.

It is possible to compute the multipoles generated by this current line as follows:

$$C_n = -\frac{\mu_0 I}{2\pi R_{ref}} \left(\frac{R_{ref}}{\mathbf{R}} \right)^n$$

where we see that a single current line generates multipoles of all orders.

Exercise – prove that the multipoles of a current line are given by the above expression.

We take the expression for the field of a current line and we write it as follows:

$$\mathbf{B} = \frac{\mu_0 I}{2\pi} \frac{1}{\mathbf{s} - \mathbf{R}} = -\frac{\mu_0 I}{2\pi} \frac{1}{\mathbf{R}} \frac{1}{1 - \left(\frac{\mathbf{s}}{\mathbf{R}} \right)}$$

the last term in the above equation can be expanded in series as follows:

$$\frac{1}{1 - \left(\frac{\mathbf{s}}{\mathbf{R}} \right)} = \sum_{n=1}^{\infty} \left(\frac{\mathbf{s}}{\mathbf{R}} \right)^{n-1}$$

and we can finally write the magnetic field using the above result:

$$\mathbf{B} = -\sum_{n=1}^{\infty} \frac{\mu_0 I}{2\pi R_{ref}} \left(\frac{R_{ref}}{\mathbf{R}} \right)^n \left(\frac{\mathbf{s}}{R_{ref}} \right)^{n-1}$$

where the product of the first two terms in the sum can be identified to be equal to C_n .

As we will see later, it is in addition often necessary to compute the field generated at a location \mathbf{s} by a magnetic moment of strength $\mathbf{m} = m_y + i m_x$ in the complex plane and located at a position $\mathbf{R} = R_x + i R_y$. The magnetic field is given by:

$$\mathbf{B} = -\frac{\mu_0 \mathbf{m}^*}{2\pi (\mathbf{s} - \mathbf{R})^2}$$

while the associated multipoles are given by:

$$C_n = -n\mu_0 \frac{\mathbf{m}^*}{2\pi R_{ref}^2} \left(\frac{R_{ref}}{\mathbf{R}} \right)^{n+1}$$

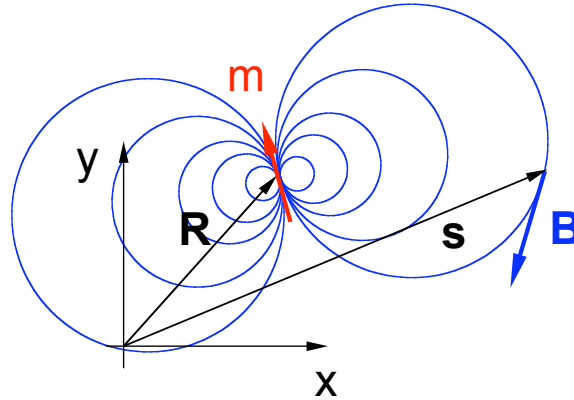


Figure 7. Field produced by a magnetic moment \mathbf{m} placed at a position \mathbf{R} in complex plane.

Most superconducting accelerator magnets are enclosed in an iron yoke which increases the field and shields the exterior from the intense magnetic field. In the case of an ideal, round iron yoke with radius R_{iron} , centered with the origin of the coordinate system and large permeability μ the effect of the iron can be computed using the method of images. For a current line of module I and located at \mathbf{R} the image current has a module I' and is placed at a radius \mathbf{R}' obtained from:

$$I' = \frac{\mu - 1}{\mu + 1} I$$

$$\mathbf{R}' = \frac{R_{iron}^2}{\mathbf{R}^*}$$

For a magnetic moment \mathbf{m} located at \mathbf{R} it is also possible to compute the image in the iron shell. The position of the image is the same \mathbf{R}' already computed, and the strength and direction of the image magnetic moment is obtained from:

$$\mathbf{m}' = -\frac{\mu - 1}{\mu + 1} \frac{R_{yoke}^2}{\mathbf{R}^2} \mathbf{m}^*$$

Associated field and multipoles are computed adding the contribution of this image current to the physical one.

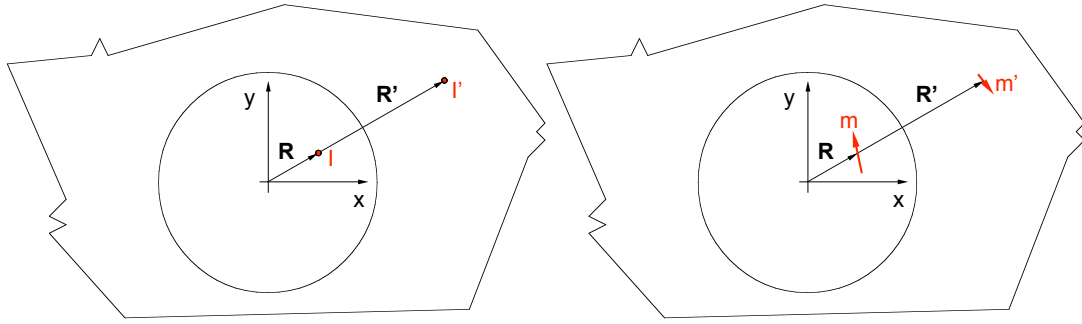


Figure 8. Image of current (left) and of magnetic moment (right) in a circular iron yoke.

Magnetic design

Magnets of a desired order can be built by a proper arrangement of the current in space, so as to produce a given multipole while cancelling other selected multipoles. The simplest current distribution that generates a pure multipole is the so called $\cos(\theta)$ arrangement. In this arrangement the current is distributed on a circle of radius R with a cosinus current density given by:

$$J = J_0 \cos(p\theta)$$

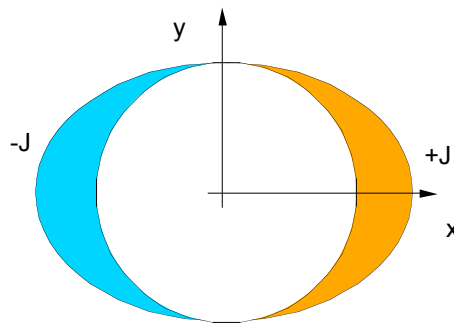


Figure 9. Schematic $\cos(p\theta)$ current distribution, with $p = 1$.

The field generated inside the circle can be computed as the integral of all elementary contributions and is given by:

$$\mathbf{B} = -\frac{\mu_0 J}{2} \left(\frac{R_{ref}}{R} \right)^{p-1} \left(\frac{\mathbf{s}}{R_{ref}} \right)^{p-1}$$

where we recognize that a $\cos(p\theta)$ current distribution generates a pure normal multipole of order p and strength:

$$B_p = -\frac{\mu_0 J_0}{2} \left(\frac{R_{ref}}{R} \right)^{p-1}$$

Similarly a $\sin(p\theta)$ arrangement of the type:

$$J = J_0 \sin(p\theta)$$

produces a pure skew multipole of order p and strength:

$$A_p = \frac{\mu_0 J_0}{2} \left(\frac{R_{ref}}{R} \right)^{p-1}$$

Exercise – show that the $\cos(p\theta)$ and a $\sin(p\theta)$ current distribution on a circle of radius R produce pure normal and skew multipoles.

We consider the $\cos(p\theta)$ distribution and we take the elementary contribution of a current element of extension $d\theta$ on the circle of radius R , given by:

$$dI = J_0 \cos(p\theta) R d\theta$$

and we compute the multipole contribution generated by this current element located at the complex position $\mathbf{R} = R e^{i\theta}$:

$$dC_n = -\frac{\mu_0}{2\pi R_{ref}} \left(\frac{R_{ref}}{\mathbf{R}} \right)^n dI = -\frac{\mu_0}{2\pi R_{ref}} \left(\frac{R_{ref}}{R e^{i\theta}} \right)^n J_0 \cos(p\theta) R d\theta$$

simplifying and integrating over the circle we obtain:

$$C_n = \int dC_n = -\frac{\mu_0}{2\pi} \left(\frac{R_{ref}}{R} \right)^{n-1} J_0 \int_0^{2\pi} [\cos(n\theta) - i \sin(n\theta)] \cos(p\theta) d\theta$$

The integral of the trigonometric functions has the following known results

$$\int_0^{2\pi} \cos(n\theta) \cos(p\theta) d\theta = \pi \delta_{np}$$

$$\int_0^{2\pi} \sin(n\theta) \cos(p\theta) d\theta = 0$$

and we therefore obtain that

$$C_n = B_n = \begin{cases} -\frac{\mu_0 J_0}{2} \left(\frac{R_{ref}}{R} \right)^{p-1} & \text{for } n = p \\ 0 & \text{for } n \neq p \end{cases}$$

We now consider the $\sin(p\theta)$ distribution and we proceed in the same way. The elementary current is:

$$dI = J_0 \sin(p\theta) R d\theta$$

that, once integrated, produces the following multipoles:

$$C_n = \int dC_n = -\frac{\mu_0}{2\pi} \left(\frac{R_{ref}}{R} \right)^{n-1} J_0 \int_0^{2\pi} [\cos(n\theta) - i \sin(n\theta)] \sin(p\theta) d\theta$$

The integral above can be solved using the additional known result:

$$\int_0^{2\pi} \sin(n\theta) \sin(p\theta) d\theta = \pi \delta_{np}$$

leading to:

$$C_n = iA_n = \begin{cases} i \frac{\mu_0 J_0}{2} \left(\frac{R_{ref}}{R} \right)^{p-1} & \text{for } n = p \\ 0 & \text{for } n \neq p \end{cases}$$

The current density distribution above is clearly not practical to wind magnets., that require the use of cables of finite size. A useful result is however achieved considering two cylinders of radius R with uniform current density J in z direction and placed along the x axis with the centers at a distance d so that they intersect. The cylinders have current in opposite direction, and the intersecting region is current free. In this case the magnetic field generated in the current-free region is uniform and it is given by:

$$\mathbf{B} = B_y = -\frac{\mu_0 J d}{2}$$

The field generated by this configuration is therefore a perfect normal dipole. A skew dipole can be obtained intersecting two cylinders placed along the y axis.

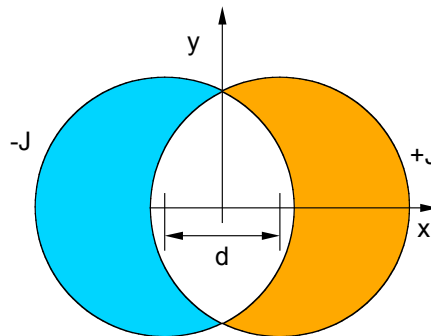


Figure 10. Schematic of the current distribution obtained intersecting two cylinders.

Exercise – prove that two intersecting cylinders generate a pure dipole field in the current-free region.

To prove this we compute the field at a point P placed inside both cylinders. The rightmost cylinder has a uniform positive current density J , while the leftmost cylinder has a uniform, negative current density $-J$. To simplify the calculation we use the vector representation of the field. The point P is located at distance d_1 with respect to the center of the leftmost circle, and distance d_2 with respect to the center of the rightmost circle. The point is at an height h with respect to the axis passing through the two centers.

For the field calculation we make use of the fact that the contour integral of the magnetic field along the boundary Γ of a simply connected surface S is equal to the flux of the current density through the surface S :

$$\oint_{\Gamma(S)} B d\Gamma = \mu_0 \int_S J dS$$

Taking as the surface S the circle coaxial with the center of the rightmost circle, and radius r_1 , the field from the first circle has constant strength and direction tangent to the circumference at all points. At the point P we have therefore that the two components of the magnetic field are:

$$B_x^1 = -\frac{\mu_0 J h}{2}$$

$$B_y^1 = -\frac{\mu_0 J d_1}{2}$$

For the second circle we use the same method and we can write that at the same point the magnetic field is

$$B_x^2 = \frac{\mu_0 J h}{2}$$

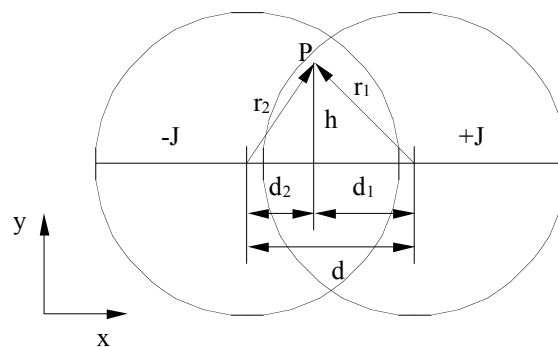
$$B_y^2 = -\frac{\mu_0 J d_2}{2}$$

The total field at P is therefore:

$$B_x = B_x^1 + B_x^2 = 0$$

$$B_y = B_y^1 + B_y^2 = -\frac{\mu_0 J d_1}{2} - \frac{\mu_0 J d_2}{2} = -\frac{\mu_0 J d}{2}$$

The only non-zero field component is directed along y , and the field does not depend on the position, i.e. it is a perfect normal dipole.



It is worth noticing that other remarkable cases can be obtained intersecting ellipses, and in particular a perfect quadrupole can be obtained intersecting two ellipses with major axes normal to each other. Similar, more relevant results, are obtained using sectors with constant current density as shown below. Although sector current distribution cannot produce a pure multipole, and contains necessarily other

multipoles as error terms, the error content can be minimised by a proper choice of the extension of the sector or using multiple sectors compensating each other.

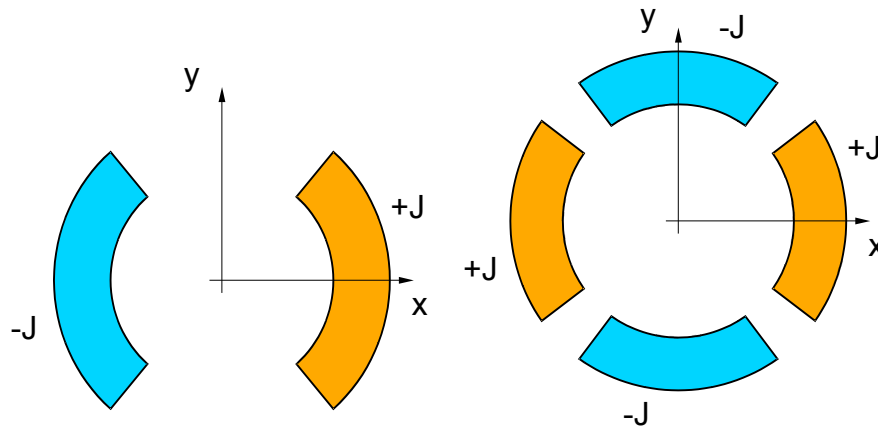


Figure 11. Sector current distribution that generates a dipole field (left) and a quadrupole field (right).

All magnetic configurations examined so far have strong symmetry. In general a perfectly symmetric multipole magnet of order m is such that the geometry of the winding and iron is rotationally symmetric by the angle π/m . After such a rotation we obtain an identical magnet if in addition we invert the current direction. This symmetry leads directly to restrictions on the orders that are *allowed* in the multipole expansion. In particular the allowed multipoles for a magnet of order m are only those that have order n :

$$n = m(2k + 1)$$

where k is an integer. For the dipole the series of allowed multipoles is therefore

$$n = \{1, 3, 5, 7, \dots\}$$

while for a quadrupole the series of allowed multipoles is:

$$n = \{2, 6, 10, 14, \dots\}$$

In addition accelerator magnets are usually produced and positioned so that they generate a pure normal or skew multipole of order m . A normal multipole magnet has top-bottom symmetry in the geometry and current. As a consequence the magnetic field on the midplane has strictly y direction. This implies immediately that the imaginary (*skew*) part of *any* allowed multipole coefficient must be zero. Similarly a skew magnet has top-bottom symmetric geometry and antisymmetric current. In this case the field on the midplane has x direction, so that all allowed coefficients have zero real (*normal*) part. The result is that in a perfectly symmetric *normal* multipole magnet only the *normal allowed* multipoles are present, and similarly for a perfectly symmetric *skew* multipole magnet, where only *skew allowed* multipoles are present.

Exercise – prove that the allowed harmonics in a perfectly symmetric magnet of order m are $n = m(2k + 1)$.

We can express the symmetry condition on a general harmonic coefficient C_n by writing that:

$$C_n' = C_n e^{in\frac{\pi}{m}} = -C_n$$

where the primed coefficient indicates the value of the harmonic after rotation and we have used a known property of the rotation of reference frame on the harmonic coefficients. The condition can be satisfied only when:

$$e^{in\frac{\pi}{m}} = -1$$

or alternatively

$$\cos\left(n\frac{\pi}{m}\right) + i\sin\left(n\frac{\pi}{m}\right) = -1$$

Equating the real and imaginary part in the above relation we can write that:

$$\cos\left(n\frac{\pi}{m}\right) = -1$$

$$\sin\left(n\frac{\pi}{m}\right) = 0$$

that is satisfied when the argument of the trigonometric functions is equal to π or its multiples of 2π . We can therefore write the condition as

$$n\frac{\pi}{m} = 2k + \pi$$

where k is an arbitrary non-negative integer number. This relation is verified for all n such that:

$$n = m(2k + 1)$$

Magnet construction

For reasons of electrodynamic and thermal stability, technical superconducting materials presently in use are manufactured in the form of twisted multifilamentary strands. The common choice for accelerator magnets is to cable the strands in flat, keystone cables, of the so called *Rutherford* type. These cables offer the advantage of high compaction fraction with minimal distortion and degradation of the superconducting strand, good mechanical stability and well controlled geometry satisfying the strict requirements for the accurate placement of conductors necessary for field homogeneity. These cables achieve high operating current density in the range of 300 to 500 A/mm².

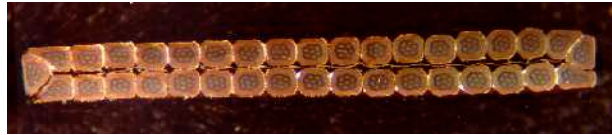


Figure 12. Cross section of a Rutherford cable

The flat Rutherford cables are wound in layers consisting of several compact conductor blocks, that can be assumed with uniform current density. The blocks are separated by wedges. The arrangement of the conductor in the blocks and of the blocks in the coil is optimised to achieve the desired field homogeneity. As an example we report the cross sections of the coils for the LHC dipole and quadrupole, with the flux lines showing the direction of the magnetic field in the bore and in the coil.

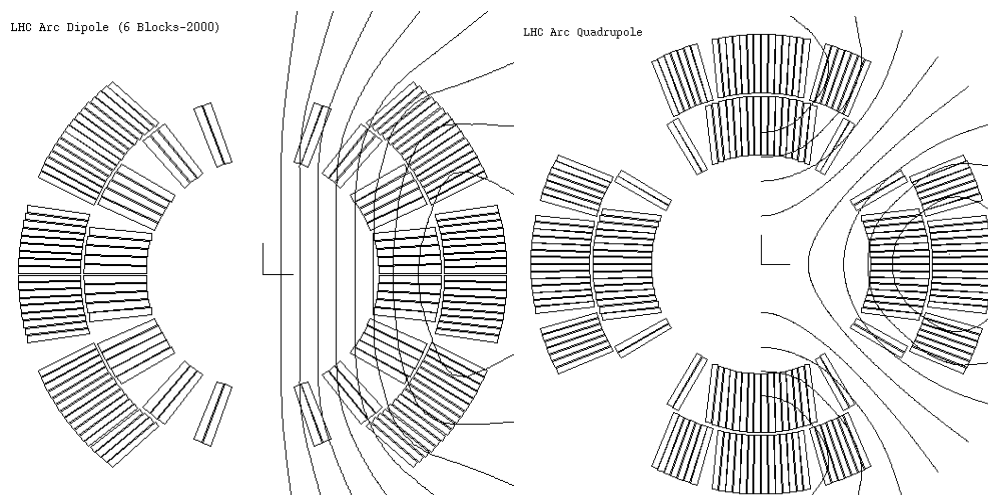


Figure 13. Cross section of the coil of the LHC dipole (left) and of the LHC quadrupole (right).

Under operating conditions the coils are subjected to a large Lorentz force. In the first quarter of the coil the electromagnetic force acts in positive direction along x , trying to explode the coil, and negative y direction, squeezing the conductors towards the midplane. In the case of the LHC dipole the electromagnetic force for a quadrant at nominal field (8.33 T) is 170 tonnes/m in x direction and -85 tonnes/m in y direction. The large structural loads are sustained by steel or aluminium collars that pre-compress and constrain the coils.

The design of accelerator magnets varies strongly depending on the objective, the available manufacturing technology and design choices. Examples of the different dipole magnet cross sections developed and built for the major superconducting accelerator projects are given below. In the case of the LHC, the collared coil assembly is surrounded by a massive iron yoke that on one hand closes the magnetic circuit, and on the other hand provides additional structural strength transmitting the load to an external steel cylinder. The outer cylinder provides leak tightness for the helium bath (subcooled, 1.9 K and 1 bar superfluid helium). Cooling is assured by a heat exchanger located in the iron yoke. The magnet is enclosed in a thermal shield and in a cryostat that provide vacuum tightness and completes the unit.

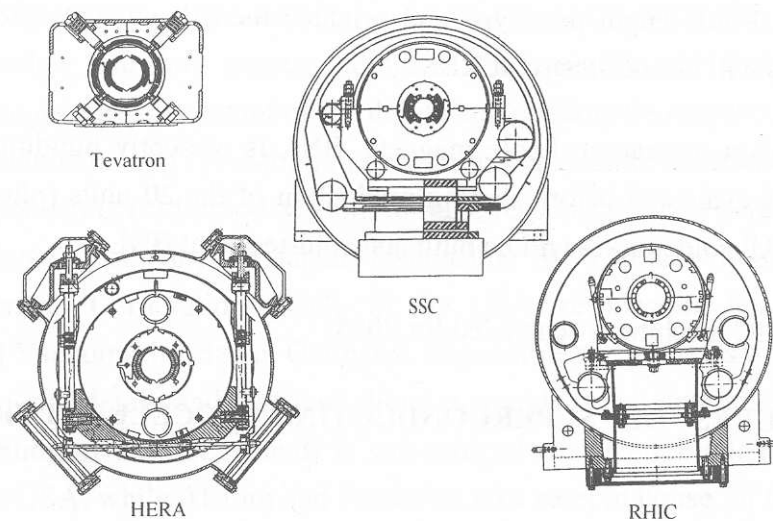


Figure 14. Cross section of the superconducting dipole magnets for large particle accelerators built or developed so far.

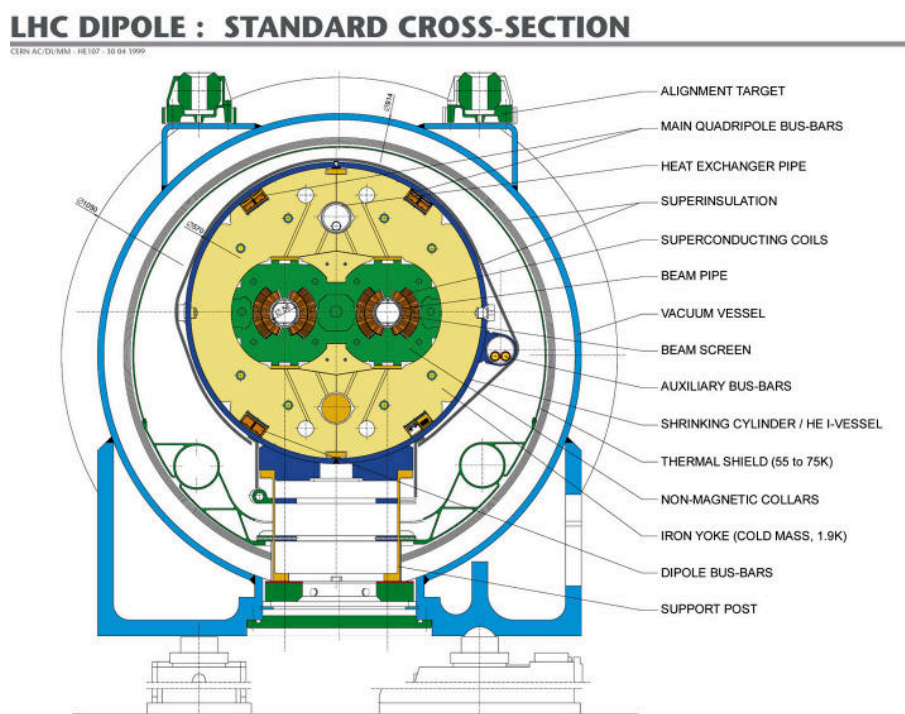


Figure 15. Cross section of the LHC dipole.

Magnetic behaviour of superconducting cables

For accelerator magnets it is very important to know and control the contribution of the superconducting cable to the magnetic field. In general terms any superconductor behaves as a diamagnetic material. In accelerator magnets the field changes are usually normal to the strands and cables and uniform along the magnet length, so that it is sufficient to consider the case of uniform normal field variations, neglecting the small errors due to the real strand orientation in a cable. We assume in addition uniform cable properties. The resulting magnetization is also normal to the strand and

cable, and has opposite direction to the field change. For purely normal magnetization we can obtain the magnetic moment \mathbf{m} associated with the unit volume magnetization \mathbf{M} simply multiplying this last by the cross section of the cable.

Three sources of magnetization are relevant for accelerator magnets:

- persistent currents in the superconducting filaments
- coupling currents in the strands, and
- coupling currents in the cables.

Persistent currents. We can compute analytically the magnetization due to the screening currents in a cylindrical filament, assuming that the critical current has a negligible variation within the filament. If the external field changes in a cyclic regime, each time reversing completely the screening current patterns, we obtain that the change ΔM of the module of the magnetization \mathbf{M} after a field change ΔB is [Wilson-83, Carr-83]:

$$\Delta M = \frac{4\mu_0}{3\pi} \lambda J_c D \left[1 - \left(1 - \frac{\Delta B}{2B_p} \right)^3 \right] \quad \text{for } \Delta B \leq 2B_p$$

in the penetration phase, until the maximum trapped magnetization is reached:

$$M = \frac{2\mu_0}{3\pi} \lambda J_c D \quad \text{for } \Delta B > 2B_p$$

after full penetration. The *first* penetration field (for *virgin* initial state) is given by:

$$B_p = \frac{\mu_0 J_c D}{\pi}$$

and full penetration is obtained in *non-virgin* state after a field change twice as large. Above we have used J_c for the field dependent critical current density and D for the filament diameter. The factor λ is the ratio of superconductor in the strand cross section, appearing because we have referred the magnetization to the unit volume of the cable (we neglect for simplicity voids in the cable).

Strand coupling currents. The filaments in a single strand are electromagnetically coupled [Wilson-83], meaning that magnetic flux changes transverse to the strand induce eddy currents that circulate in the superconducting filaments and close resistively across the strand matrix. Coupling currents are established and decay with a characteristic time constant τ that depends on the twist pitch of the filaments in the strand l_p and on the matrix (effective) transverse resistivity ρ_{eff} . For NbTi strands used in accelerator magnets this time constant is of the order of 10 ms.

Assuming that the coupling currents are fully established (i.e. for ramp times much larger than the time constant τ of the currents), the module of the magnetization M of a circular superconducting strand subjected to a transverse field change \dot{B} is given by [Wilson-83]:

$$M = \frac{\mu_0}{\rho_{eff}} \left(\frac{l_p}{2\pi} \right)^2 \dot{B}$$

proportional to the ramp-rate.

Cable coupling currents. A superconducting, flat cable for particle accelerator magnets responds to field changes in a manner similar to the filaments in a strand. In this case the superconducting strands themselves are coupled. Coupling currents flow along the strands and cross-over at the points where the strands touch each other. We can identify at least two such type of contacts, namely that of crossing strands, touching in a point, and that of adjacent strands, touching ideally along a line. It is customary to characterize the contacts through two resistances, referred to a single contact of two strands, the transverse R_c and the adjacent R_a resistances.

In the case of a homogeneous field variation \dot{B}_\perp normal to the wide face of an infinitely long cable with constant contact resistances a convenient expression for the magnetization associated to fully established coupling currents is [Wilson-72]:

$$M \approx \mu_0 L_p \left[\frac{(N^2 - N)}{120} \frac{\alpha}{R_c} + \frac{N^2}{96} \frac{1}{\alpha R_a} \right] \dot{B}_\perp$$

where N is the number of strands, α is the aspect ratio of the cable (ratio of width to thickness) and L_p is the cable twist pitch. The first term in brackets is originated by coupling currents closing at the crossing of strands, while the second term is due to currents closing on adjacent strands. We see at once that as in general $\alpha \gg 1$, the second term can be neglected when the transverse and adjacent contact resistances are of the same order of magnitude. Under the same assumptions above, for a uniform field variation \dot{B}_\parallel normal to the thin face of the cable the magnetization is given by:

$$M \approx \mu_0 L_p \left[\frac{N^2}{128} \frac{1}{\alpha^3 R_a} \right] \dot{B}_\parallel$$

Exercise – estimate the order of magnitude of the magnetization of an LHC cable for the main bending dipoles. The main characteristics of this cable are reported in table 1 below. For LHC particle injection is foreseen at 0.54 T. The highest ramp-rate on the cables is of the order of 7 mT/s, of which we can take approximately 5 mT/s for both components normal and parallel to the broad face.

Magnetization in the superconducting filaments will be largest at the lowest field levels (when the critical current density is large). At the injection field the NbTi has a critical current density in the range of 20,000 A/mm². The calculation is therefore performed at injection conditions.

If we compute the magnetization components as discussed in the previous sections we obtain:

• filaments magnetization	14	(mT)
• filaments coupling currents	0.3	(mT)
• cable magnetization normal to the broad face	3.1	(mT)
• cable magnetization normal to the thin face	0.001	(mT)

We see clearly that for this typical conductor design and operating conditions the dominant magnetization is due to the filament persistent currents. Generally, in the range of cable parameters given above, the magnetization due to coupling currents within the strand, and the cable magnetization due to field changes normal to the thin face of the cable are negligible.

Main properties of the LHC strand and inner layer cable.

Strand				
Diameter	d	(mm)	1.065	
Copper:NbTi ratio		(-)	1.6	
Filling factor	λ	(-)	0.38	
Filament size	D	(μm)	7	
Twist pitch	l_p	(mm)	25	
Critical current density	J_c			
at 0.5 T, 1.8 K		(A/mm ²)	≈ 20000	
at 8 T, 1.8 K		(A/mm ²)	≈ 2000	
Cable				
Number of strands	N	(-)	28	
Cable dimensions				
thin edge	h_1	(mm)	1.72	
thick edge	h_2	(mm)	2.06	
width	w	(mm)	15.0	
Aspect ratio	α	(-)	7.9	
Twist pitch	L_p	(mm)	110	
Cross contact resistance	R_c	($\mu\Omega$)	≈ 10	
Adjacent contact resistance	R_a	($\mu\Omega$)	≈ 10	

Field errors in accelerator magnets

A systematic approach to the magnetic field analysis in an accelerator magnet is to break the total field generated in the bore into its components of different origin. We can identify for steady state operation the following field components:

- *geometric*, related to the cable positions in the winding pack, the accuracy of their placement and movements during energization;
- *iron magnetization*, accounting for the magnetization and saturation of the iron yoke as a function of the excitation field;
- *persistent currents*, originating from the contribution of the magnetization of the superconducting filaments to the field.

The first two geometric and iron magnetization are purely static and are proportional to the excitation current. The third, the persistent current magnetization, is in principle also of steady state nature, but can show a long term variation as will be discussed later on. The persistent currents magnetization has a large hysteresis that appears as a difference in the ramp-up and ramp-down branches of the magnet loadline at low excitation. These three contributions, in the case of a *perfect* magnet, will appear only on *allowed* harmonics, i.e. those permitted by the symmetry conditions of the coil. As already discussed, this is evident for symmetric geometry. If the iron geometry and superconductor properties also respect the magnet symmetry conditions, the resulting magnetizations, both for iron and superconductor, will have the same degree of symmetry and thus will only contribute to allowed harmonics.

An example of the three different contributions in steady state can be clearly seen in the measurement of normal sextupole in a superconducting dipole as shown in Fig. 1. We have plotted there the transfer function (ratio of field to current) of the normal dipole and the sextupole components as measured in steady state conditions at different levels of current during the ramp-up and ramp-down in an LHC dipole. The average value of both multipoles for ramp-up and -down is constant for fields below approximately 5 kA, according to the linear contribution associated to the winding geometry. Above 5 kA we see that the average of the transfer function strongly deviates from a constant owing to the iron saturation. The superconductor magnetization is responsible for the hysteresis in the two curves at low field. The field dependence of the magnetization is clearly visible.

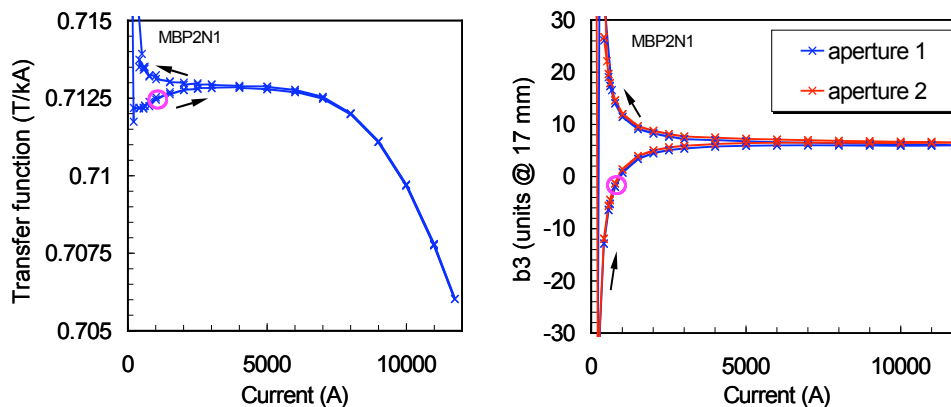


Figure 16. Transfer function of the normal dipole (left) and normal sextupole (right) for a LHC prototype dipole. The circle indicate injection condition (760 A). Nominal operating field is reached at 11850 A.

In addition to the above contributions, it is possible to observe in accelerator magnets the following effect of dynamic nature:

- *coupling currents*, due to the ramp-rate dependent magnetization in the superconducting strands and cables;
- field *decay* during constant current plateaux and *snapback* at the start of the ramp.

As discussed above, the cable magnetic moment originating from coupling currents is proportional to the field ramp-rate and inversely proportional to the transverse strand and cable resistances. In fact the ramp-rate magnetization is mainly associated with the field change normal to the broad face of the cable. The effect of coupling currents is a constant additional hysteresis for a given ramp-rate over the whole field range.

The interstrand resistance of the cable is known to depend critically on several factors, among them the surface conditions of the strands, their ageing, heat treatment conditions during coil fabrication, and possibly the electromagnetic pressure on the strand contacts at operation. Hence in a coil we can have an arbitrary distribution of interstrand resistances along the magnet length and within the winding cross section. This distribution does not necessarily respect the geometrical symmetries. The consequence is that the magnetization can vary on a cable-by-cable basis within the

winding and in principle all harmonics can be present at ramp, as shown above by the existence of a non-zero normal quadrupole.

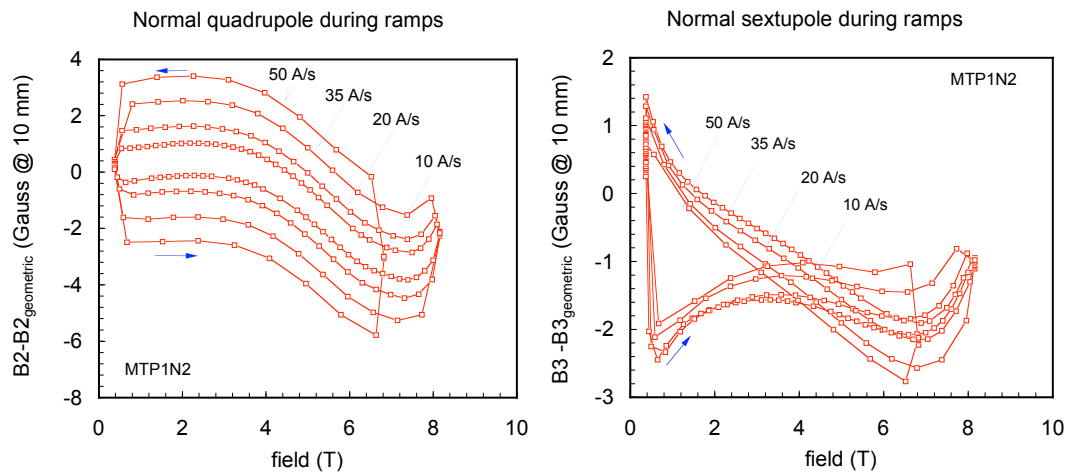


Figure 17. Measurement of normal quadrupole and normal sextupole during ramps at increasing ramp-rates, in an LHC prototype. Both quadrupole and sextupole are given here in non-normalised terms to show the constant shift of the steady ramp-up and -down branches.

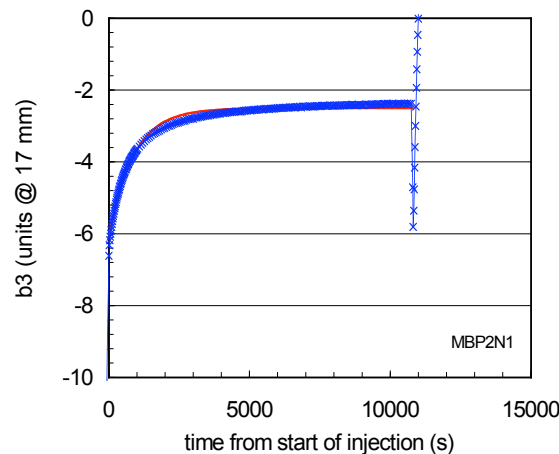


Figure 18. Decay of the sextupole in a LHC prototype and subsequent snap-back.

The decay and snap-back is a phenomenon that was unexpected and surprising during the first operation of the Tevatron collider. It was deduced then from the evidence of large chromaticity drifts, or *decays*, during periods when the excitation current of the magnets was constant. At the restart of ramping, after the plateau, the sextupole returned to its original value in a few seconds. This sextupole *snap-back* could be observed in the Tevatron through collateral effects, such as emittance blow-up and beam losses. Tables were generated based on independent magnetic measurements of dipole magnets and used in Tevatron to cope with the variations of chromaticity. It was found then that the sextupole drift at injection is increased pre-cycling the magnet at high operating current, increasing the duration of the precycle flat-top or repeating the pre-cycling procedure several times before the measurement. In summary, the magnet has a *memory* of the previous powering history. This memory can be erased only quenching the magnet.

The nature of the field decay can be explained as an interaction among current distribution in the cable and persistent current filament magnetization. Any change of current distribution in a cable is associated with a periodic variation of the local magnetic field (mostly the self-field) along the cable. In turn any field variation causes a change in the magnetization state of the superconducting filaments. Because of the non-linear response of the superconductor magnetization to changes in the external field, the net change of the magnetization of the filaments is always in the direction of a decreasing absolute value of the average cable magnetization. This indeed explains the systematic drift of the allowed multipoles in the direction of decreasing magnetization contribution. The diffusion of the current profile in the cable has very long time constants which are coherent with the characteristic times observed on the field drift (hundreds of seconds and above). Finally, the internal field changes necessary to explain the drift of the harmonics observed is small, in the range of 10 mT. Such a field change can be generated in a typical Rutherford cable for accelerators by a current redistribution among strands of some 10 A, a value which also coherent with the expected current imbalances, e.g. generated by the localised field variations discussed in the previous section.

Bibliography

References to the material treated in this lecture can be found in the following articles and books.

- [Beth-66] R.A. Beth, *Complex Representation and COmputation of Two-Dimensional Magnetic Fields*, J. Appl. Phys, **37** (7), 2568-2571, 1966.
- [Beth-67] R.A. Beth, *An Integral Formula for Two-Dimensional Fields*, J. Appl. Phys, **38** (12), 4689-4692, 1967.
- [Brechna-73] H. Brechna, *Superconducting Magnet Systems*, Springer Verlag, Berlin, 1973
- [Carr-83] W.J.Carr, *AC Loss and Macroscopic Theory of Superconductors*, Gordon and Breach Science Publishers, New York, 1983
- [Devred-01] A. Devred, *Superconducting Magnets for Particle Accelerators and Storage Rings*, in *Engineering Superconductivity*, P.J. Lee ed., John Wiley & Sons, 2001
- [Mess-96] K.-H. Mess, P. Schmueser, S. Wolff, *Superconducting Accelerator Magnets*, World Scientific, 1996.
- [Schmueser-91] P. Schmueser, *Superconducting Magnets for Particle Accelerators*, Rep. Prog. Phys., **54**, 1991, 683
- [Wilson-72] M. Wilson, *Rate Dependent Magnetization in Flat Twisted Superconducting Cables*, RHEL Internal Report, RHEL/M/A26, 1972
- [Wilson-83] M. Wilson, *Superconducting Magnets*, Clarendon Press, Oxford, 1983